

# Extremely Large Telescope Prefocal Station A system concept

S.A.E. Lewis<sup>1</sup>, E. Brunetto, A. Förster, C. Frank, I. Guidolin, S. Guisard, P. Hammersley, R. Holzlöhner, P. Jolley, J. Kosmalski, U. Lampater, E. Marchetti, P. La Penna, T. Pfrommer, P. Zuluaga  
European Southern Observatory, Karl-Schwarzschild-Str. 2, 85748 Garching bei München,  
Germany;

## ABSTRACT

The Prefocal Station (PFS) is the last opto-mechanical unit before the telescope focal plane in the Extremely Large Telescope (ELT) optical train. The PFS distributes the telescope optical beam to the Nasmyth and Coudé instrument focal stations and it contains all of the sky metrology (imaging and wavefront sensing) that will be used by the active optics of the telescope and to support operations such as phasing the primary mirror (phasing and diagnostic station). It also hosts local metrology that will be used for coarse alignment and maintenance. We present the main results of a concept design study for the Nasmyth A prefocal station.

**Keywords:** ELT, wavefront sensing, active optics, segmented mirror phasing, Nasmyth platform

## 1 INTRODUCTION

The Prefocal Station (PFS) is the last opto-mechanical unit before the telescope focal plane in the Extremely Large Telescope (ELT) optical train; one PFS will be installed on each Nasmyth platform. The main functions of the PFS are (1) distributing the telescope optical beam to three Nasmyth focal stations and the Coudé train (2) optical sensing to support low-order optimization and seeing-limited image quality (3) optical sensing to characterize telescope subsystems (4) hosting coarse alignment metrology. PFS-A has been broken down into a PFS-A Main System and several hosted units (cameras, phasing and diagnostic station, metrology). ESO has overall system responsibility for PFS-A; the PFS-A Main System will be designed and produced by IDOM S.A.U.; the other hosted units will be developed by ESO together with industrial suppliers. Presented here are the results of a concept design study for Prefocal Station A performed internally at ESO. One of the main goals of the study was to define and validate requirements for the PFS-A Main System and the hosted units.

The PFS provides its wavefront sensing functions in the context of an ELT wavefront control scheme that is organised into three layers: blind, low-order optimization and adaptive optics. These layers are described briefly in the following sections. System requirements for PFS-A have been used as the basis for a concept design study of PFS-A, the main purpose of which was to define and validate requirements for the PFS-A Main system and the other hosted units. The system requirements, an overview of the concept design, and some of the main results from performance analysis and validation activities at ESO are also reported here. The concept design is described in overview and reference is made to previous reports [3,4] for further details of the mechanical design and the sensor arm.

It is expected that, during the detailed design phase, the design of the PFS-A Main System and the hosted units will evolve from the initial concept described here. In particular, the teams responsible for the final realisation of these items must meet functional and performance requirements, but there is no requirement to rigidly follow the concept described here and alternative technically-compliant design solutions may be adopted.

### 1.1 System Context

Prefocal Station A is located on Nasmyth platform A of the ELT; it is the last opto-mechanical system of the telescope after M5 and before the instrument focal planes. PFS-A has an optical interface with up to three Nasmyth instruments and with the Coudé optical train. One of the functions of PFS-A is to direct the telescope science beam to the instrument that is currently observing and this will be done by reconfiguring the optics of the PFS. PFS-A is also required to perform optical sensing functions to support telescope active optics and to characterise key subsystems such as the

---

<sup>1</sup> slewis@eso.org; phone +49 89 32006931; www.eso.org

segmented primary telescope mirror. The role of the PFS-A optical sensing within the overall telescope control scheme is shown in Figure 1; it can be regarded as a wavefront sensor that works in conjunction with a controller and several actuators: the telescope mirrors and main structure. Consistent with this approach, system requirements for the PFS-A optical sensing have been formulated in terms of wavefront sensing performance rather than overall system performance.

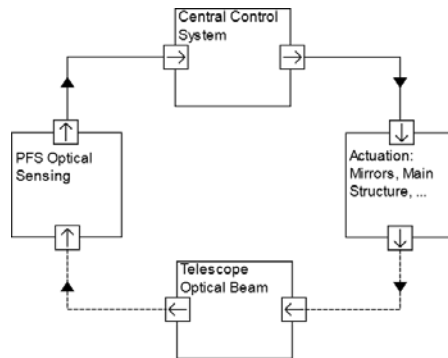


Figure 1: PFS Optical Sensing Context

## 1.2 Wavefront Control Context

The wavefront control required to observe with the ELT is organized in three control layers: blind control layer, low-order optimization (LOO), and adaptive optics. In addition, offline optical sensing functions are required for telescope and subsystem characterisation.

The blind control layer relies on internal metrologies and look-up-tables to compensate the large amplitude distortions of the main structure under gravity and thermal load. The M1 figure is corrected in real time with position actuators controlling the segments positions in piston, tip and tilt. This is based on the signals of edge sensors monitoring in real time the relative displacements of adjacent segments. The M2, M3 and M4 units are controlled in position at slow rate against their internal metrologies with set points extracted from look-up tables. The performance of the blind layer determines the entrance conditions for the PFS-A optical sensing at acquisition. At acquisition, immediately after a blind pointing, PFS-A will observe the following image errors [1]:

- a pointing error of up to 10 arc seconds (radius);
- a geometric spot diameter of up to 3 arc seconds;
- dynamic tip/tilt errors with an RMS amplitude of around 1 arc second;
- dynamic focus, coma and astigmatism with a combined wavefront error amplitude of a few microns.

The LOO layer corrects the quasi-static aberrations (one correction every 5 minutes including times when adaptive optics is running) observed by the Natural Guide Star (NGS) optical sensing at the PFS-A adapter and manages the distribution of strokes between the internal degrees of freedom of the ELT. The wavefront measurements from the PFS are made in the presence of the time-evolving telescope errors and instrument adaptive optics corrections applied to M4.

The third layer, the adaptive optics, relies on resources distributed throughout the telescope (M4 adaptive mirror, M5 fast tip-tilt correction, laser guide star (LGS) projectors) and post focal instruments and AO modules (LGS Sensing, NGS sensing including tip/tilt and low-order wavefront).

The offline optical sensing to characterise telescope subsystems is used to find the set point of the M1 segment edge sensors by means of the PFS-A Phasing and Diagnostic Station (PDS) that is served by the M6 Coudé mirror. The PDS will be used at several stages in the telescope lifecycle including initial alignment during assembly, integration and verification (AIV), commissioning, maintenance and routine characterization of the telescope during operations. A suite of different sensors, performing guiding, high and low order wavefront sensing, as well as phasing tasks, in the visible and near infrared, are designed for that purpose and installed directly underneath the Coude focus on the Nasmyth platform. The entrance conditions for the M1 phasing characterization will range from M1 being mechanically aligned (initial alignment), segments stacked and brought to coherence (AIV and commissioning, maintenance) and segments phased to within tens or a few hundreds of nm (normal operation).

### 1.3 PFS-A System Requirements

This section summarises some of the main system requirements for PFS-A which will be permanently installed on the ELT and operate in the telescope dome environment. A functional breakdown structure of PFS-A is given below:

- Optical beam propagation
  - Direct a beam to the three Nasmyth foci
  - Direct a beam to the Coudé train
- Optical sensing to support acquisition
- Optical sensing to support guiding
- Optical sensing to support low order optimisation
- Optical sensing to support seeing limited operation
- Optical sensing to support characterisation of telescope subsystems
  - M1
    - Phasing
    - Scalloping
  - M2-M5 active control functions
  - M4 phasing
- Hosting optical metrology equipment

PFS-A shall propagate the telescope science field of view to any of the three Nasmyth focal stations and to the Coudé optical train. The full 5 arc minute radius telescope field of view shall be transmitted to the straight-through Nasmyth-A focus (denoted A1); an unvignetted field for view of 2.25 arc minutes radius shall be transmitted to the lateral Nasmyth foci (denoted A2 and A3); an unvignetted field of view of 30 arc seconds radius shall be transmitted to the PDS and the Coudé optical train entrance. PFS-A may obstruct the annular part of the telescope optical beam from 2.5 arc minutes to 5 arc minutes radius to perform its optical sensing functions. The quasi-static wavefront error introduced onto the telescope science beam by the PFS-A optics shall not exceed 60nm RMS and the total induced dynamic tip/tilt error shall not exceed 0.4 mas RMS in the frequency range 1 to 100Hz.

For acquisition, PFS-A shall record images of the telescope focal plane in the wavelength range 800-950nm with a field of view of 10 arc seconds radius at rates up to 10Hz. PFS-A shall measure guiding images at user-selectable frequencies up to 500Hz with position measurement errors of the guide star not exceeding 10 mas RMS provided that the following conditions are fulfilled:

- low order optimisation is running;
- seeing conditions are better than 1 arcsec;
- an NGS brighter than  $m_R = 15$  can be used by the PFS-A optical sensing.

To support low order optimisation, PFS-A is required to measure the following focal plane characteristics using natural guide stars at three points in the telescope field of view:

- focus;
- the wavefront aberrations from Noll Zernike 5-11 inclusive (reference [2]) at frequencies up to 1Hz;
- the positions of the three NGS images with respect to each other (plate scale and focal plane tip/tilt).

For seeing-limited operation, the maximum sensed Zernike Noll order is 100 with an allowed measurement error of 250nm RMS for all measured orders (excluding piston, tip and tilt) combined. The allowed total guiding measurement error is 50mas RMS for this use case.

The above optical sensing requirements also apply during non-sidereal tracking and during small offsets of the telescope pointing with an amplitude not exceeding 10 arc seconds on sky.

The requirements for characterising telescope subsystems are still preliminary. At the time of writing, these requirements are being validated and defined in more detail in the frame of a test-bench activity called MELT (reference [6]) and they will manifest themselves in the requirements for the phasing and diagnostic station (PDS) in the course of the next 12 months. As described earlier, the functional requirements cover different phases of the ELT lifecycle from initial alignment through to maintenance, troubleshooting and routine characterisation during operation. The broad areas of application are:

- supporting AIV and the commissioning of the ELT;
- maintenance, troubleshooting, and routine characterisation during operation including:

- characterising and trouble-shooting the adaptive functions of the telescope;
- aligning and maintaining the segmented primary mirror.

In terms of performance, the measurement errors of the M1 phasing steps once the system has been brought into operation shall not exceed 50nm optical path difference.

Finally, PFS-A is required to host metrology that will be used to characterize and maintain the PFS, to align instruments to the telescope and for general telescope maintenance. The metrology imposes requirements on the PFS for:

- interfaces, volume and supply of services for the metrology measuring devices;
- line of sight to the sensor arms;
- line of sight to M5 and the M6 mirror units;
- permanently installed metrology targets.

## 2 PFS-A DESIGN DESCRIPTION

This section contains a description of a concept design for PFS-A that was developed to derive and validate requirements for the PFS-A Main System and the other hosted units (camera systems, phasing and diagnostic station, metrology). It is expected that the design will evolve from this initial concept during the detailed design phase, and it is not mandatory for the groups responsible for the detailed design and production to rigidly follow this concept provided that the functional and performance requirements are met.

### 2.1 Product Breakdown

The product breakdown structure for PFS is shown below in Figure 2; the responsibility for each item is also indicated. The PFS-A Main System is the main part and it includes the mechanical structure, both M6 mirror units, a natural guide star adapter equipped with three sensor arms, local control system and auxiliary equipment. The M6N mirror is deployed into the science beam to serve the lateral Nasmyth foci and the M6C mirror feeds the Coude optical train and the PDS. The NGS adapter sensor arms provide wavefront sensing during science observation using light picked off from the annular technical field surrounding the science beam.

The requirements related to characterising the telescope and subsystems (particularly the primary mirror) have been allocated to the PDS, which is a subsystem of PFS-A. The PDS will use the 30 arc second radius optical beam reflected from the M6C mirror as described above and be mounted on the Nasmyth platform floor at a gravity invariant location.

The imaging camera system and the wavefront sensing camera system will be used in the corresponding imaging and wavefront sensing channels of the sensor arm. The same camera type may also be used in the PDS. The phasing camera system or systems will be used in the PDS for telescope subsystem characterisation tasks. A camera system includes the detector, front-end electronics and all the necessary supporting infrastructure and control system necessary to realise a fully tested and verified turn-key camera system.

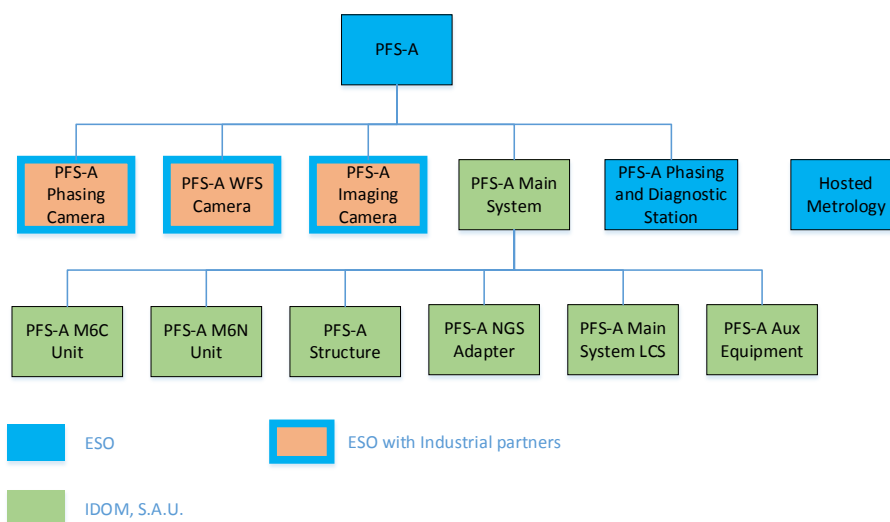


Figure 2: PFS-A Product Breakdown Structure

## 2.2 PFS-A Overall Mechanical Design and Structure

A PFS-A mechanical concept design is shown in Figure 3 and mounted on the ELT main structure in Figure 4. The mechanical design and some of the trade-offs were already reported in detail in reference [3]. The overall dimensions of PFS-A are 5m wide x 4.75m deep x approximately 10m high. The common framework structure provides mechanical support for the hosted units and the mechanical interface to the Nasmyth platform. The selected design is a welded steel structure with a mass of approximately 8900kg that interfaces with the Nasmyth platform at four interface points in the corners of the system footprint. The NGS adapter is mounted as a single module on attachment points on the common framework structure. The common framework structure also provides interface attachment points for hosted metrology and an access path for the Nasmyth platform crane to the PDS. Some of the requirements for the common framework structure include:

- Maximum permitted mass;
- High stiffness;
- Survival during earthquake;
- Maximum reaction forces exerted on the Nasmyth platform during earthquake;
- Stable support for hosted units;
- Access to hosted units;

A preliminary mechanical finite element analysis performed using ANSYS Workbench, with the system loaded up to its maximum allowed 40000kg total mass with all subsystems, resulted in the performance listed in Table 1.

**Table 1: PFS-A Mechanical Performance**

Characteristic	Value
1 <sup>st</sup> three eigenfrequencies (Hz)	9.16; 11.77; 14.26
Earthquake Nasmyth interface reaction forces Fx (kN) max/min	636.1 / -595.1
Earthquake Nasmyth interface reaction forces Fy (kN) max/min	350.4 / -349.2
Earthquake Nasmyth interface reaction forces Fz (kN) max/min	1106.4 / -1404.1

PFS-A is required to comply with its functional and performance requirements in the presence of several external input perturbation sources. In addition to temperature variations throughout the night and wind, these error sources include small amplitude vibrations of the telescope structure at the Nasmyth platform interface and slow mechanical distortions of the Nasmyth platform interface points. Vibrations are analysed and budgeted at ELT system level in the frequency range 1-110 Hz.

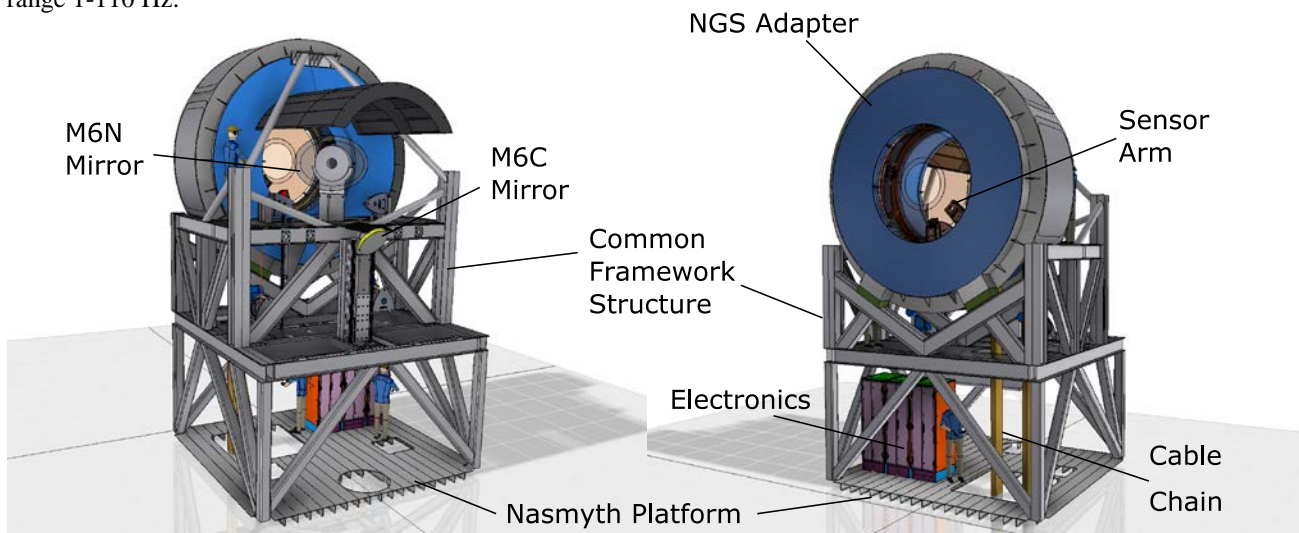


**Figure 3: Prefocal Station A main system mechanical concept with the M6N mirror deployed into the optical beam (A2 focus configuration) with some of the main subsystems identified. Left: PFS-A viewed from the primary mirror side; Right: PFS-A viewed from the Nasmyth platform side.**

Distortions of the Nasmyth platform interface points are expected, particularly during Azimuth rotation, due to small imperfections of the telescope structure and can be characterised as scaling and shearing of the interface pattern both in-plane and out-of-plane. Although the amplitude of the distortions is small, of order 0.25mm, this error source is an important constraint on the design of the PFS-A common framework structure and the M6 mirror units.



**Figure 4: 3D sketch of the Prefocal Station on the ELT Nasmyth platform.**

### 2.3 NGS Adapter

The PFS-A requirements for optical sensing to support acquisition, guiding and field stabilisation, low order optimisation, and seeing limited image quality are allocated to the NGS adapter. Shown in Figure 3 in blue, it is a modular circularly-shaped 5m diameter subsystem mounted on the common framework structure with the help of position-adjusting devices that will be used to align it to the ELT mechanical altitude axis. The NGS adapter comprises three sensor arms, a cable wrap system, and a mechanical structure.

Three sensor arms are shown mounted on the NGS Adapter structure in Figure 5. Each sensor arm will normally pick off a different natural guide star in the telescope field between 2.5 and 5 arc minutes (497mm to 995mm radial), leaving the field inside 2.5 arc minutes unvignetted. The pickoff plane is located 1440mm before the natural ( $f/17.7$ ) telescope focus. Independent radial and rotational motion of the sensor arms is required to allow a wide range of asterisms of three NGS to be sensed simultaneously, subject to a minimum angular separation limit of 45 degrees between the arms. A total angular rotation range of 540 degrees has been specified to allow the NGS adapter to track the sky rotation. The cable wrap system serving the three sensor arms, shown in Figure 6, comprises a primary hanging cable loop having a rotation range of 540 degrees and two secondary cable wraps providing 120 degrees rotation range relative to the primary sensor arm.

The required position measurement errors of the sensor arm focal plane image with respect to the NGS adapter mechanical supporting structure were derived from the system requirements using a Monte-Carlo analysis considering randomly-selected NGS asterisms. The analysis showed that a position measurement error at the focal plane of  $175\mu\text{m}$  RMS is sufficient to measure the distance between two stars with an error of 0.03% with a confidence level of 95% in a mixed statistical interpretation. The dynamic NGS position measurement error specified in section 1.3 corresponds to a total error (root square sum of the tip and tilt axes) of  $\leq 33\mu\text{m}$  RMS when translated into mechanical performance.

### 2.3.1 Sensor Arm Design Description

A possible opto-mechanical concept for the sensor arms was already reported in detail in reference [4] and is illustrated in Figure 7. A flat mirror will pick-off the telescope light (20 arc second on-sky field), and direct it to the optical box. The optical box contains the optics for both imaging and wavefront-sensing optical paths; the imaging path forms an image conjugated with the telescope focal plane on the imaging camera detector surface; the wavefront sensor path (WFS) forms an image of the telescope pupil on the lenslet array of a Shack-Hartmann wavefront sensing camera. The imaging path will receive the light in the wavelength range of 800-950nm, while the WFS will work in the 500-800 nm range. The wavelengths are separated by a dichroic mirror. The sensor arm also provides the following functionality:

- compensation of the telescope non-telecentricity by tilting the pick-off mirror;
- refocusing by moving a pair of folding mirrors in a retro-reflector configuration;
- field stop;
- pupil lateral position actuation;
- variable neutral density filters;
- internal calibration light source;
- box shutter to close the optical box and make it light tight;

with each sensor arm having a designed mass of around 270 kg before weight reduction.

For the WFS camera system, a new detector currently in development will be used. The detector will have 800×800 pixels, on a 24 μm pitch, for a total detector area lateral dimension of 19.2 mm. The mean readout noise of the WFS is specified to be 3 electrons RMS with an excess noise factor of 1.0. For the imaging camera system, it is planned to use a deep depletion CCD 220 camera [5], with good sensitivity in the red. The CCD 220 has 240×240 pixels, each with 24 μm side, for a total detector lateral dimension of 5.76 mm. The optical design is driven by the detector specifications. In the imaging path, the whole 20 arcsecond ( $\pm 10$  arc second radius) field must be contained on the detector area, implying a focal surface diameter of 5.76 mm and a pixel scale of 83mas/pixel. On the WFS path the pupil must be about 10% smaller than the detector, resulting in a telescope pupil image of about 17 mm diameter at the exit of the sensor arm optical box.

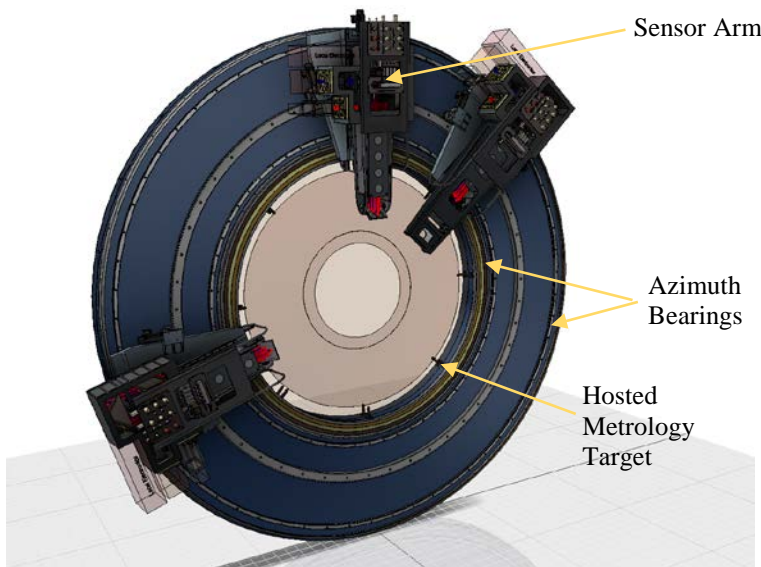
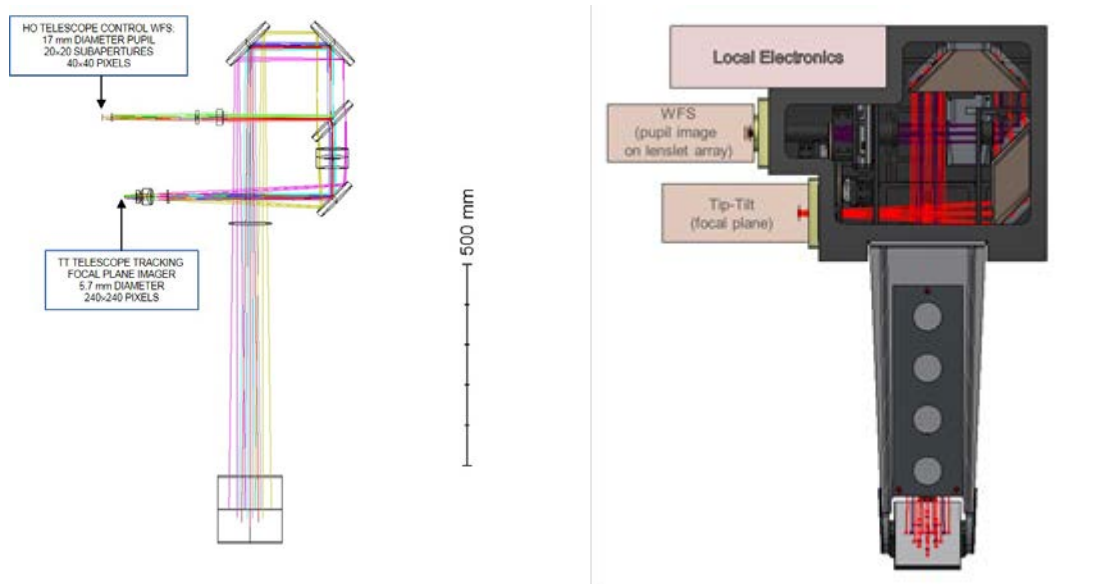


Figure 5: NGS Adapter: Sensor Arms and Supporting Structure



Figure 6: NGS Adapter: Cable Wrap System



**Figure 7: Left: optical drawing of the Sensor Arm. Right: optomechanical concept.**

The main requirements for the imaging and wavefront sensing channel optics are summarized in Table 2 and Table 3.

**Table 2: Imaging channel main requirements**

Focal Plane Imaging Optics Requirements	
Parameter	Value
Wavelength range	800-950nm
Field of View	20 arc seconds (diameter)
Pixel scale	83 mas/pixel with 24 $\mu$ m pixels
Radius at 80% EE (on axis)	$\leq 4.8$ pixels diameter ( $\leq 0.4$ arcsec on sky)
Plate scale difference between X and Y	<0.3%

**Table 3: Wavefront sensing channel main requirements**

Wavefront Sensing Requirements	
Parameter	Value
Wavelength range	500-800nm
Pupil diameter	17mm (708 pixels)
Wavefront Sensor Type	Shack Hartmann (20x20 sub-apertures)
Pixels per sub-aperture	35pix
Sub-aperture Unvignetted Field of View	4 arc seconds (diameter)
Pupil blur	<3% of a sub-aperture
Wavefront error Z5 to Z11 combined	<35 nm RMS
Wavefront error Z5 to Z100 combined	<60 nm RMS

The optical design reported in reference [4] delivers, in the imaging channel, a nominal polychromatic ensquared energy diameter of approximately 2 pixels at centre field and a plate scale linearity of better than 0.2% in both X and Y directions. In the wavefront sensing channel, the pixel scale is 0.3 arcseconds per pixel which gives adequate sampling of the best-expected seeing. The maximum pupil blur for an off-axis field point never exceeds 7% of a subaperture (at the edge of the pupil, less than 5% close to the center) [4]. For the on-axis field, the maximum (chromatic) blur is smaller than 3%. The total wavefront error (that is, including all the modes up to Z37, also focus) is plotted in Figure 8 and is essentially diffraction limited over the entire field in the central wavelength range, and it never exceeds 70 nm RMS.

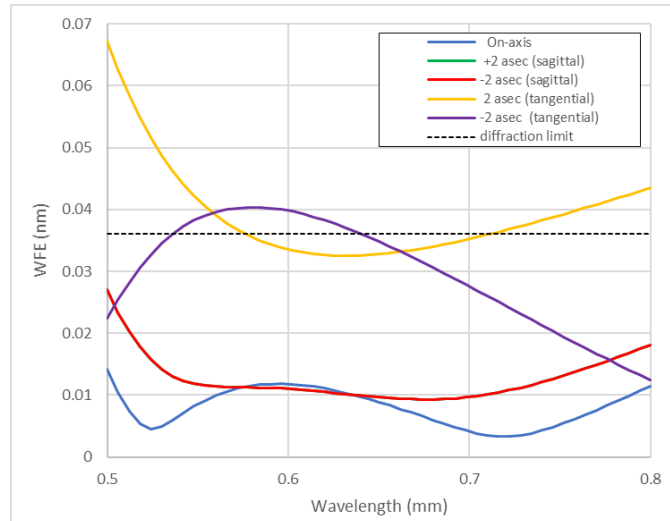


**Figure 8: Plot of the nominal wavefront error (SA centered on 3.75 $\mu$ m on-sky) versus wavelength for various field points. The wavefront is mostly diffraction-limited with an error always less than 70 nm RMS.**

The mechanical eigenfrequencies of the sensor arm were calculated by applying a rigid boundary condition at the interface between the sensor arm azimuth-rotating structure and the azimuth bearing. The first six eigenfrequencies were found to be local modes of the cable guide with a relatively small moving mass fraction; the first eigenfrequency with a substantial mass participation was found to be at 65.5Hz as shown in Figure 9.

### 2.3.2 Sensor Arm Performance Analysis

The performance of the sensor arms is specified in terms of constraints on knowledge errors, i.e. actual performance can be improved by appropriate calibration algorithms. Requirements were defined to constrain static and dynamic knowledge errors of one sensor arm both for the imaging and the wavefront sensing, as well as the relative position between sensor arms.

Results derived with an integrated model (see Section 3 for details) indicates that quasi-static knowledge errors of the sensor arm are dominated by gravity deformations, as well as interface deformation at the mechanical interface with the Nasmyth platform and temperature gradients. The modelling results indicate that reaching compliance with the concept design is feasible. The dynamic requirements are more stringent and dominant error sources are centroiding on faint stars and stick-slip effects due to friction that impact the tracking quality of the sensor arm. While friction does not play a role at most tracking speeds, it can become crucial at very low speeds close to the Stribeck velocity. Since friction can have a significant impact on performance, it must be looked at in detail during further design phases. A breadboard will be developed to validate the proposed drive system design.

A critical parameter for the optical design is the pupil motion introduced by the error sources. This is specified as an absolute performance error and constrained to be not larger than  $\pm 5\%$  of the diameter of the Shack-Hartman lenslets which corresponds to  $42\mu\text{m}$  distance at the pupil image. The dominant error source is found to be sensor arm motion due to stick-slip effects when the sensor arm is moving at low speeds close to the Stribeck velocity, but compliance can be reached.

A full report on the performance analysis is beyond the scope of this document, however two examples of the performance error analysis contributions are described in a little more detail in the following sections. These are:

1. The effect of variable gravity direction;
2. Camera measurement noise.

### 2.3.3 Sensor Arm Gravity-Introduced Performance Errors

The optical performance errors of the sensor arms under varying gravity load direction were evaluated by combining optical sensitivity matrices with the calculated rigid-body displacements of the optical elements. Sensitivity matrices were calculated from the optical design using the new ESO in-house software tool Sensitizer [7]; finite element analysis

was performed using ANSYS. The analysis included the following optical performance errors, the first four of which correspond to System requirements:

- Pointing error in the imaging (tip/tilt) channel;
- Focus error in the wavefront sensing channel;
- Total wavefront error from Z5 to Z11 inclusive in the wavefront sensing channel;
- Total wavefront error from Z5 to Z100 inclusive in the wavefront sensing channel;
- Pupil position error in the wavefront-sensing channel.

With the sensor arm at its worst0-case maximum radial extension, 2 arc minutes off axis, the pointing error of each sensor arm was found to vary by  $\pm 20$ mas in the direction perpendicular to the sensor arm base plane over a full rotation of the sensor arm with the pointing error in the orthogonal in-plane direction varying by  $\pm 11$  mas. The pointing errors are consistent with the required values given at the start of section 2.3.

The focus error in the wavefront sensing channel (Noll Z4) was found to vary by  $\pm 27$  nm over the full rotation range. The focus error is consistent with the System requirement of  $\pm 43$  nm stated in section 1.3. The RMS wavefront errors at centre-field from Z5 to Z11 combined were negligible on-axis for the gravity load case.

The pupil position error in the wavefront sensing channel was found to vary by  $\pm 29$   $\mu$ m in the direction perpendicular to the sensor arm base plane and  $\pm 20$   $\mu$ m in the orthogonal direction over a full rotation. This is less than  $\pm 5$  % of the Shack-Hartmann sub-aperture size of 850  $\mu$ m and in any case substantially smaller than the inherent motion of the telescope exit pupil; it is concluded that this error source represents no additional constraint on the operation of the PFS.

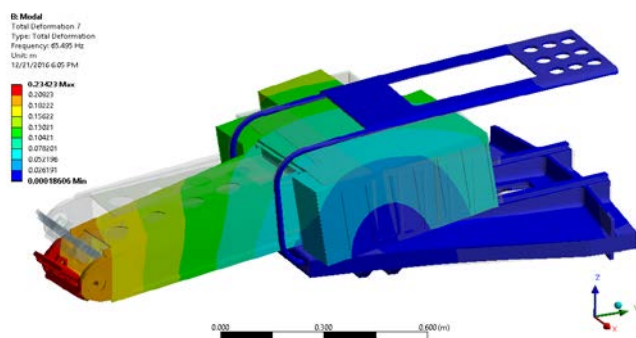


**Figure 9: Sensor arm lowest eigenfrequency with a substantial moving mass fraction (ie. excluding local modes of the cable guide).**

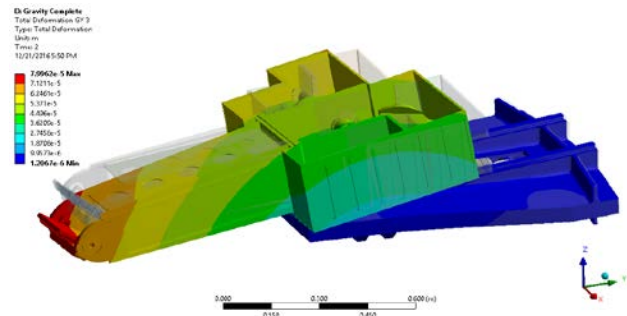


**Figure 10: Sensor arm displacement with gravity acting in the -Y direction.**

### 2.3.4 Sensor Arm Camera Measurement Error Performance

Performance estimates for the imaging and wavefront sensing cameras were made using the camera quantum efficiency, pixel scale, read noise and dark current, telescope and sensor arm optical transmission, atmospheric seeing and sky background. Effects that have not been included in the calculation are scintillation caused by atmospheric turbulence and the influence of the atmospheric outer scale on low-order wavefront estimation (primarily focus). In the results presented here, simple centroiding, weighted-centre-of-gravity and a matched filter were used to estimate the spot positions on the detectors.

In the imaging channel, the full telescope aperture is imaged to a single spot and the sub-aperture centroid error can be directly compared with the position measurement error requirements. Figure 11 shows the calculated centroiding error (temporal RMS) when measuring at 200 Hz with the full moon 25° away from the science target for four different seeing values. The solid curves correspond to simple centroiding, dotted to weighted centre of gravity, and dashed to matched filter centroiding. The lower horizontal dashed line represents a centroid error of 9.2mas RMS consistent with the required fast guiding measurement errors. The upper dashed line corresponds to a temporal RMS error of 50 mas, required for seeing-limited imaging.

For the wavefront sensing channel, a modal reconstruction assuming sub-apertures in both square and circular grid arrangements with 20x20 samples over the pupil was used. Table 4 contains the conversion factors from sub-aperture

slope errors,  $\sigma_{sl}$ , to global spatial average WFE in the given set of Zernike modes for both square and circular grids. The errors in the circular grid are slightly lower, supposedly because the edges of the pupil are evenly covered with sub-apertures, whereas the square grid leaves open areas.

**Table 4: Conversion factors from sub-aperture slope rms errors to Zernike RMS errors for square and circular Shack-Hartmann sub-aperture geometry**

Zernike Mode Range	Number of modes in estimator	square grid factor [nm/mas]	circular grid factor [nm/mas]
4	1 to 11	1.2	1.2
5–11	1 to 11	2.9	2.8
5–11	1 to 106	4.0	3.5
5–79	1 to 79	5.7	5.4
5–106	1 to 106	8.5	7.0

The sub-aperture RMS slope errors (temporal RMS) for the wavefront sensor camera are plotted in Figure 12 for exposure times of 60s, 30s, 1/20s and 1/200s for centre of gravity, weighted-centre-of-gravity and matched-filter centroiding. The most conservative conditions in terms of sky-background, observing 25° away from the full moon, are considered in this calculation; this becomes a performance limitation for fainter guide stars. The three, horizontal black dashed lines in the figure correspond to:

- Lower line: focus measurement error equal to  $\pm 375 \mu\text{m}$  (corresponding to user-required Z4 error of  $< \pm 43 \text{ nm}$ );
- Middle line: total spatially-averaged wavefront error up to Noll Zernike 106 of 250 nm RMS;
- Upper line: guiding measurement error of  $< 50 \text{ mas}$  RMS (relevant for seeing limited operation).

The system requirement of 125 nm RMS total wavefront error in Zernike modes 5–11 for LOO corresponds to a sub-aperture slope error of 43 mas (not indicated in Figure 12).

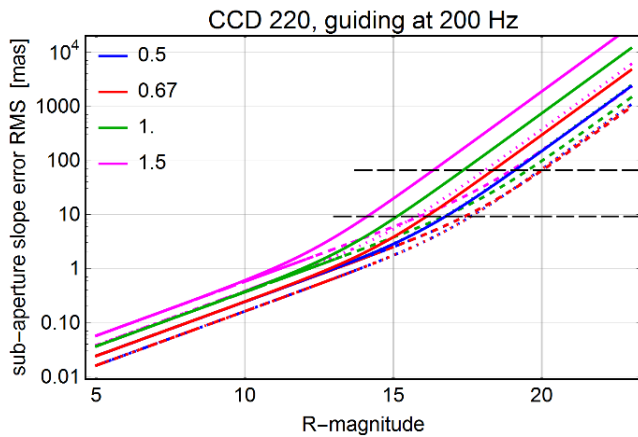


**Figure 11: Imaging Channel wavefront sub-aperture slope error (temporal RMS) at full Moon 25° at four different seeing values. Solid (dotted) curves: (W)CoG, dashed: matched filter.**

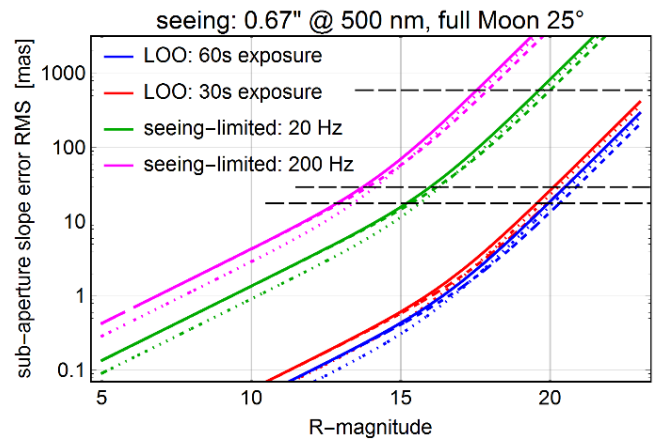


**Figure 12: Wavefront sensor sub-aperture slope error (temporal RMS) at full Moon 25° at four different exposure times. Solid (dotted) curves: (W)CoG, dashed: matched filter. Left: Seeing 0.67", right: 1.0"**

PFS-A is required to meet all performance requirements over at least 95 % of the sky accessible to the telescope over telescope altitude angles from  $+30^\circ$  to  $+88.5^\circ$  and  $360^\circ$  in azimuth. Computations using randomly selected NGS asterisms and the Besançon galaxy model show that, for the three NGS configuration, this can be obtained with natural guide star asterisms where the faintest star has a magnitude of at least  $m_R=19$  with the other two stars typically being significantly brighter. From the above data, it can be concluded that (1) the wavefront sensor measurements to support low order optimisation (focus and low-order aberrations up to Z11) would not be limited by camera system measurement noise (within the assumptions made here) due to the large telescope aperture and relatively long measurement times (2) for the seeing-limited use case, a total WFE of  $< 250 \text{ nm}$  RMS for the first 100 Noll Zernike modes (measured by a single sensor

arm) can be achieved for a measurement rate of 20Hz with a  $m_R=16$  star under the full moon bright-sky conditions analysed here.

## 2.4 M6N Unit

The M6N unit comprises an elliptical flat mirror with a clear aperture of 1456 mm x 1038 mm (major and minor axes) with its cell, supporting structure and deployment mechanisms. The M6N mirror unit can be deployed in two different positions to direct the central 2.25 arc minute radius portion of the telescope field to either of the A2 and A3 Nasmyth instrument focal stations; it can also be fully retracted from the telescope beam to allow the full telescope optical beam to be transmitted to the straight-through A1 focal station.

As reported in reference [3] one possible realisation of the M6N mirror unit is shown in Figure 13. The mirror is supported from the back and below by a cell and supporting structure with a rotation mechanism and vertical motion actuated using a pair of winches and guide rails. The total mass of the mirror unit is approximately 3000 kg.

The required corresponding mechanical position accuracy of the mirror positioning system (which is not the only error source) of approximately  $\pm 0.5$  mm and  $\pm 60$   $\mu$ rad tilt is achieved using commercially available kinematic seats that are designed for the high load-levels associated with an assembly of this size.

In the A2 and A3 configurations, the telescope sensor arm on-sky patrol field is limited by the shadow of the M6N mirror and its support projected to the focal plane. To minimize the shadowing, the mechanical size of M6N is limited to be not more than approximately 10 mm (radius) larger than the clear aperture; the vertical support is allowed to vignette an additional 11 % of the technical field at the telescope focal plane. With these constraints, the available patrol field for the PFS sensor arms is 31.4 square arc minutes.

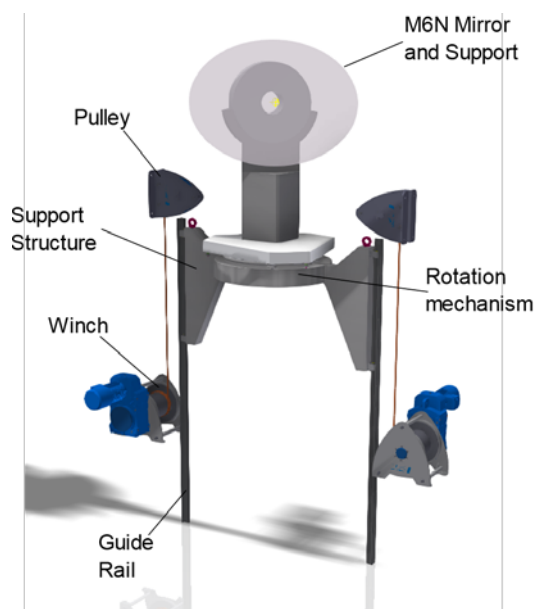


**Figure 13: M6N concept deployment system**

The clear aperture of the M6N mirror is sufficiently large to reflect the required NGS field of view of 2.25 arc minutes radius without vignetting and an LGS field of view of 1.3 arc minutes radius for an object at a distance of 80km above sea level (77km above the ELT entrance aperture) as demonstrated in the beam footprint diagrams Figure 14 and Figure 15, respectively.

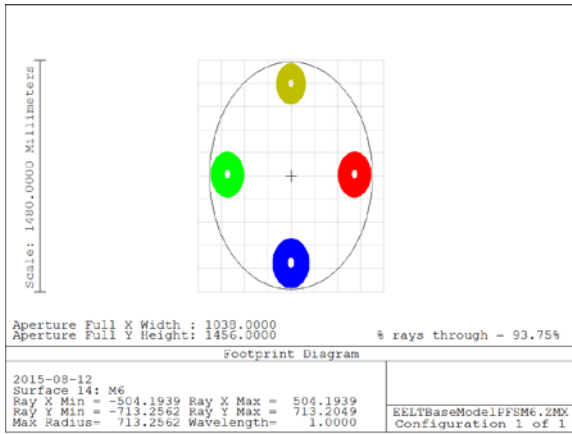


**Figure 14: Optical beam footprints on M6N for a field of  $\pm 2.25$  arc minutes in X and Y and an object at infinity.**

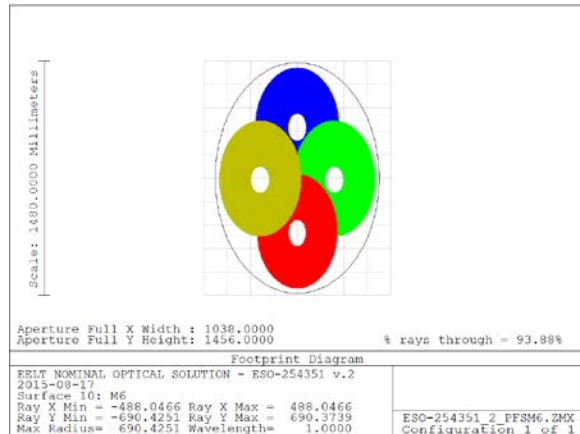


**Figure 15: Beam footprints on M6 for a point source at 80km ASL and  $\pm 1.3$  arc minutes LGS field angle in X and Y**

The M6N mirror is close enough to the focal plane for focal plane anamorphism to be a consideration. Focal plane anamorphism is defined a change of the plate scale along a single axis resulting in an anisotropic distortion of the focal surface. A preliminary analysis of the sensitivity of focal plane anamorphism to surface figure errors on the M6N mirror was made by successively applying Zernike surface sag figure errors to the mirror and calculating the focal surface distortion using a best fit to several field points. The results of this analysis are plotted in Figure 16. The amplitude of the sag perturbation in this analysis was 1 micron RMS for each Zernike order and the analysis has some limitations because the Zernike sag errors are defined on a circular aperture although the mirror is elliptical. Taking into account the actual specified figure errors of M6N, the expected plate scale anamorphism would be of order 0.2mas/arcminute although the final value will depend on how the figures are distributed over spatial frequency.

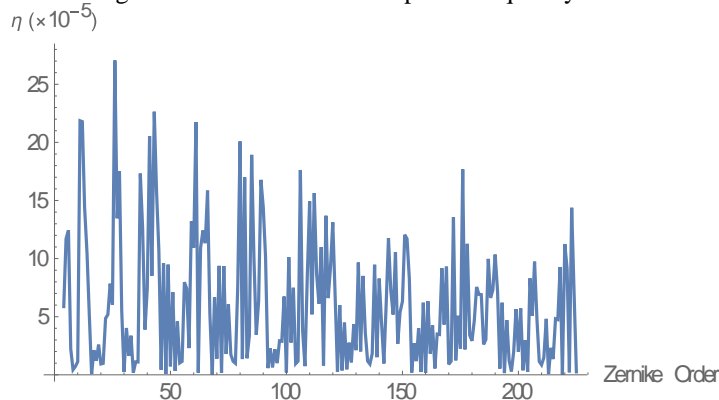


**Figure 16: Sensitivity of NGS focal plane anamorphism,  $\eta$ , to Noll Zernike surface sag errors on the surface of M6N from Z4 through to Z225. The amplitude of the sag error used for calculating sensitivity was 1 micron RMS.**

The performance requirements on lateral focal plane stability constrain the absolute position error of M6N in the quasi-static and in the dynamic frequency range. Both requirements were analysed by applying relevant disturbances to the integrated model of the PFS-A Main System including, but not limited to, the error sources mentioned previously in this section.

The main error sources contributing to the quasi-static performance are M6N position repeatability and flexible deformation of the Nasmyth platform at the mechanical interface with the PFS (the worst case being an out-of-plane astigmatic deformation). Further errors sources like temperature gradients and wind loads were analysed, but they have no significant impact on lateral focal plane stability. Note that the PFS is located in an area where wind speeds are limited to about 2 m/s by the dome windscreen. While particularly interface deformation may warrant a thorough

detailed design of the mirror support system, meeting the quasi-static performance requirements is considered feasible based on the results of this concept study.

The constraints on vibration as indicated earlier in this paper are stringent, and the absolute position error was analysed for both vibration sources external to the PFS (vibration at the mechanical interface with the Nasmyth platform), as well as potential PFS internal vibration sources. It is clear from the analysis that meeting the dynamic performance requirements will require both an optimized mirror support and minimizing internal vibration sources. The concept design is particularly sensitive to vibration in the 10-100 Hz frequency range, where amplification through structural modes plays an important role in the resulting micro-vibrations of the mirror units and sensor arms.

## 2.5 M6C Unit

The M6C unit comprises an elliptical flat mirror with a clear aperture of 691 mm x 500 mm (major and minor axes) with its cell, supporting structure and deployment mechanisms. The M6C mirror unit can be deployed into the telescope beam to direct the central part of the telescope field to the Coudé optical train entrance and the PDS; it can also be fully retracted from the telescope beam. One possible realisation of the M6C mirror unit, as reported in reference [3], is shown in Figure 17. The mirror is supported from the back and below by a cell and supporting structure with a linear stage providing vertical motion to deploy the mirror into the telescope optical beam. The total mass of the M6C mirror unit is approximately 1300 kg.

When the M6C mirror is deployed, the telescope sensor arm on-sky patrol field is limited by the shadow of the M6C mirror and its support projected onto the focal plane. The mechanical size of the mirror and its support have been designed to minimize the vignetting of the focal plane; the available patrol field for the PFS sensor arms is 40 square arc minutes when the M6C mirror is deployed.

The clear aperture of M6C is large enough to reflect a field of view for natural guide stars of 30 arc seconds (radius) without vignetting. This is larger than needed for the Coudé train, but it is expected that the full field will be used by the PDS to fulfil its imaging function. Figure 18 shows an optical diagram including M6C, the PDS and the Nasmyth platform traced for a natural guide star object at centre field. The telescope NGS focal plane is 850mm above the Nasmyth platform.

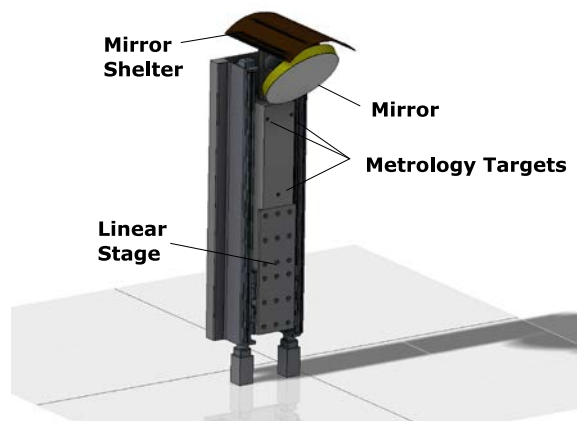


**Figure 17: M6C Mirror Unit in the out of beam configuration**

Figure 19 shows an optical layout for an on-axis laser guide star object at an altitude of 90 km above sea level and a telescope zenith distance of 45°. In this configuration, the LGS object is 123 km from the telescope entrance aperture. At this zenith distance, and larger, the footprint of the laser guide star optical beam lies comfortably within the clear aperture of M6C. The LGS focus is 3375 mm below the Nasmyth platform and the location will change with line of sight distance to the LGS in the mesosphere, and hence with telescope zenith distance.

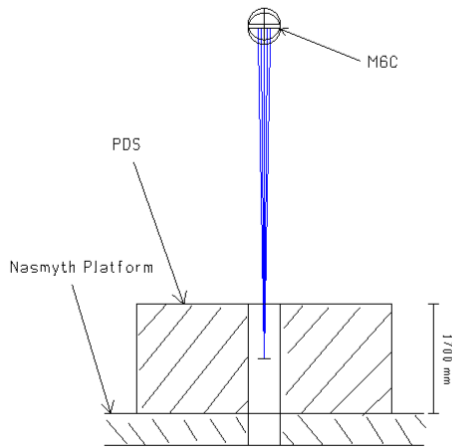


**Figure 18: NGS Focus after M6C shown together with the Nasmyth platform floor and the PDS design volume**

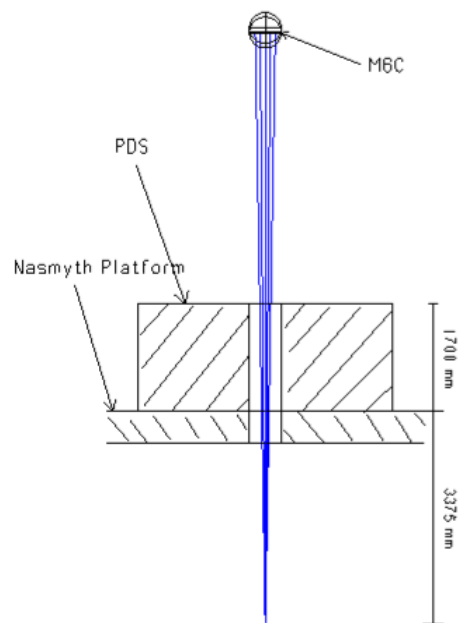


**Figure 19: LGS Focus after M6C shown together with the Nasmyth platform floor and the PDS design volume**

The absolute performance requirements on the motion of the Coudé train entrance focal plane are analogue to the ones established for the lateral focal plane. While the conclusions for the lateral focal plane presented in the previous section apply, the performance analysis revealed that the current design of M6C is very sensitive to vibration in the 10-100 Hz range. This is likely due to the boom-like design of its support, which needs to be optimized in the further design phases.

## 2.6 Phasing and Diagnostic Station

The phasing and diagnostic station (PDS) will support the following system-level tasks of ELT:

- Characterising the primary mirror
  - Segment capture
  - Segment stacking and bringing the segments into coherence
  - Segment phasing and figure control
- Characterising the active control functions of telescope mirrors and actuators other than the primary
- Wavefront sensing to support stand-alone SCAO imaging with the telescope for diagnostic purposes
- Seeing-limited imaging for diagnostic and verification purposes
- Verification of LGS functionality (still to be confirmed)

These high-level tasks will be broken down into use cases and operational scenarios as detailed requirements are developed. The development and validation of requirements for the PDS is currently being undertaken in the frame of a test-bench project called MELT (Miniscule ELT) [6]. The results of MELT will feed into the requirements and design of the PDS as they become available.

A design volume has been allocated for the PDS as a PFS hosted unit. It is located on the Nasmyth platform in the path of the Coudé optical beam; a cylindrical opening through the PDS volume is left free for the Coudé optical beam; the PDS will insert pickoff optics into the optical beam when it is used. The design volume is shown in Figure 20; it has dimensions 4000 mm wide x 1650 mm deep x 1700 mm high and the through-hole has a diameter of 500 mm.

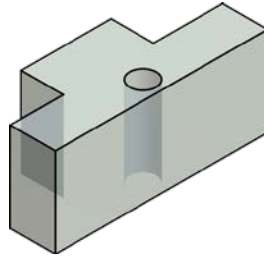


**Figure 20: PDS Design Volume; the through hole is coaxial with the Coude optical axis.**

As shown in Figure 18, the NGS focal plane of the telescope is at the level of the PDS volume and the PDS can pick off light both before and after the NGS focus. Conversely, the LGS focal plane is located significantly after the NGS focus and below the Nasmyth platform floor as shown in Figure 19 and described in the accompanying text. Both the figures mentioned here show a cross-section through the PDS design volume labelled as “PDS” in the figure.

In case the PDS is required to perform LGS wavefront sensing, it would be preferable to simultaneously observe the LGS and a NGS which raises the question of how to separate the light from the two objects. The optical beam footprint of a LGS at the NGS focal plane after M6C is shown in Figure 21 below. The ray trace was performed for an on-axis laser guide star object at an altitude of 90km above sea level and a telescope zenith distance of 45 degrees. The central clear aperture in the footprint, due to the telescope central obstruction, has a diameter of approximately 60mm, which corresponds to a NGS field of 18 arc seconds on sky. The presence of this clear aperture raises the possibility of spatially separating an on-axis NGS and an on-axis LGS (rather than using a dichroic) so that they could be simultaneously observed by the PDS.

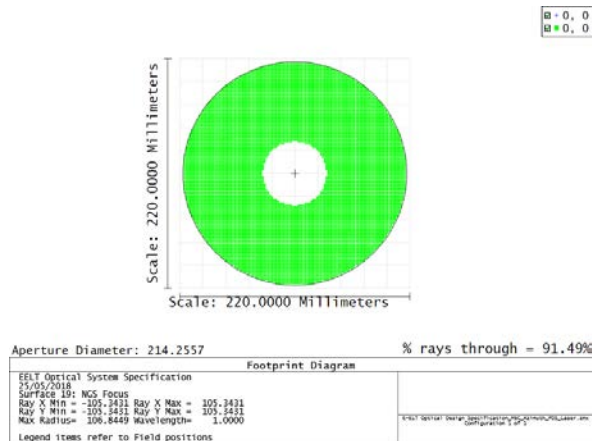


**Figure 21: Footprint diagram showing the LGS beam footprint at the level of the NGS focus after M6C. The clear central aperture due to the telescope central obstruction has a diameter of approximately 60mm**

## 2.7 Hosted metrology

PFS-A will host optical metrology that will be used for assembly, integration and verification, commissioning, and realignment during operation. In this context, hosting means providing a free design volume for installation and an access path, mechanical interfaces, and routing for supplies and services. A design volume for the hosted metrology measuring equipment has been allocated in the space between M6C and the main axis cable wrap. The metrology will be installed from above the PFS using a crane in the ELT dome. The hosted metrology design volume intersects the telescope optical beam so that the metrology measuring devices can be positioned directly on the telescope optical axis and at different locations in the field of view. From its installation location, the hosted metrology has line of sight to both M6 mirrors and the PFS sensor arms. Additionally, the metrology has line of sight to the Nasmyth instruments, imaging through the M6N mirror to the lateral foci. Finally, the metrology measuring devices can also look backwards towards M5 making measurements of the position of this unit provided that suitable targets are installed. The metrology will not be used during science observation, but rather for offline characterization tasks and there will be no potential interference

between the hosted metrology and the telescope science light. The optical metrology measuring instruments will include, in the concept elaborated here, a laser tracker and an optical sighting telescope.

The complement to the metrology measuring devices are metrology targets that will be installed on the units that will be characterized by the metrology. The following target locations are foreseen:

- PFS common framework structure
- M6C mirror support
- M6N mirror support
- M5 (to be confirmed)
- NGS Adapter structure
  - laser tracker targets
  - removeable target for sighting telescope
- Sensor arm
  - optics box
  - pickoff mirror
  - internal focal plane

It is also expected that the instruments and the phasing and diagnostic station will include targets compatible with these metrology means according to their own installation and alignment plans.

Figure 22 shows a conceptual realisation of the hosted metrology and targets for the M6C measurement configuration. The metrology is positioned at the required position using a pair of vertical linear stages and a horizontal stage to give an X-Y type motion. Three laser tracker targets are permanently installed on the mirror support structure enabling the metrology to characterize the six position rigid body degrees of freedom. A similar scheme is used to characterize the other PFS configurations: M6N and sensor arm.

The operating concept and possible measurement accuracy obtained with the sighting telescope, mounted directly adjacent to the laser tracker, will be the subject of breadboard tests in the next phase of the system design.

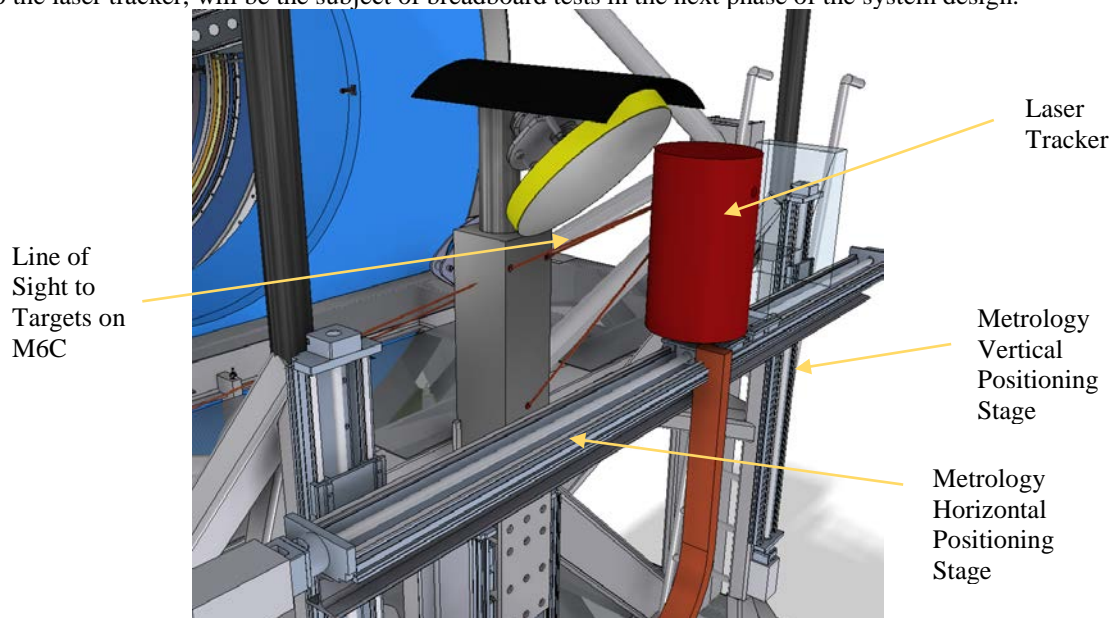


**Figure 22: PFS Hosted Metrology in the M6C configuration. The vertical and horizontal linear stages position the red laser tracker volume. Lines of sight from the laser tracker to metrology targets permanently mounted on the M6C support are also shown.**

### 3 INTEGRATED SYSTEM MODEL

An integrated model was developed to evaluate performance of the PFS system concept within its anticipated environment. Refer to Figure 24 for a block diagram of the model structure. It consists of a representative state space model of the PFS-A main structure (400 modes up to 200 Hz) with one sensor arm mounted in the top position (12 o'clock), accompanied by lumped mass representations of the two other sensor arms in the minimum 45° distance to

either side. The drive systems, such as azimuthal and radial sensor arm positioning systems, the focus trombone and the pickoff mirror positioning systems have been modelled in a simplified fashion. The model ignores for the time being the detailed drive design, but considers encoders and friction effects in the guide rails of azimuth, radial, and focus trombone drives (note the pickoff mirror will be flexure-based, and no friction model was considered in this case). The model is exposed to the external disturbances as specified in the environmental conditions. These disturbances are wind, flexible deformations at the mechanical interface of the PFS with the Nasmyth platform, as well as vibrations at this interface.

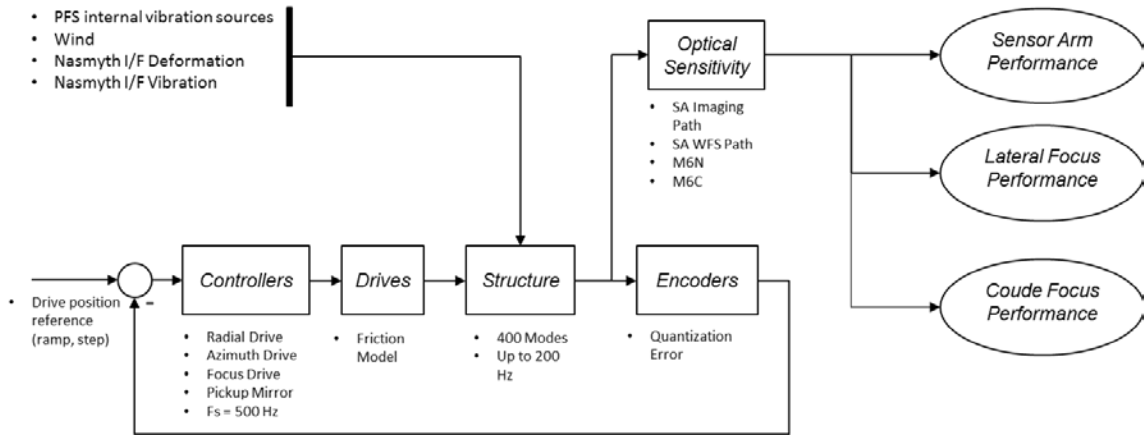


**Figure 23: Block diagram of PFS-A Main System integrated model**

Furthermore, temperature gradients (0.1 K/m) and gravity loads on the sensor arm were considered as separate static load cases outside the frame of the integrated model.

The integrated model generates displacements of optical nodes of the sensor arm in six rigid body degrees of freedom for the NGS adapter sensor arms (both imaging and wavefront sensing channels), as well as for beam propagation by the M6N and M6C mirror units. These node motions are then transformed into optical performance with the help of optical sensitivity matrices derived from the Zemax optical design using the ESO software tool Sensitizer, which is described in more detail below. The optical errors derived this way are then post-processed to yield contributions of individual error sources to relevant performance requirements.

#### 4 SENSITIZER

SENSITIZER is an ESO software toolset written in Matlab and Mathematica aiming at automating some Structural/Thermal/Optical Performance (STOP) sensitivity analyses with Zemax *OpticStudio* (ZOS). The core code of SENSITIZER runs in MATLAB and drives ZOS in the background through the ZOS-API interface, based on .NET (superseding the obsolete DDE interface). The output is saved in the MATLAB file format and can be post-processed using MATLAB and/or Mathematica routines. The optical system to analyse is defined in a normal Zemax lens file.

The core data structure of SENSITIZER is an optical *group*, which can be any optical surface in the lens file or a set of subsequent surfaces. These groups will be perturbed by varying their positions relative to the rest of the system (rigid-body-motions, RBM) and/or by adding Zernike shape deformations on their front surface. After a certain perturbation is applied, ZOS runs (sequential) raytracing to compute the optical performance such as centroid displacement or wavefront error.

SENSITIZER can run in two different modes: Either by applying perturbations separately to each group and each degree of freedom, or else by perturbing all groups in all degrees of freedom at the same time. The first mode is used to compute sensitivity matrices, the second to evaluate specific compound perturbations. Perturbations can be defined in Zemax surface coordinates or else in global coordinates, e.g. for modeling perturbations provided by a finite-element simulation.

The tool is available to the public as open-source software (GPL v.3 license) reference [7].

## 5 CONCLUSIONS

The development of a system concept for PFS-A of the ELT has been reported in overview here. This includes the development of system requirements, generation of a concept design, and performance analysis. The purpose of the concept design development was to derive and validate requirements for the PFS-A subsystems that will be designed in detail and produced in the frame of several industrial contracts and in-house developments at ESO. It was found that critical performance requirements include the precise mechanical positioning of the sensor arm opto-mechanics and mirror units in the presence of distortions of the Nasmyth platform interface and vibrations (particularly of the large mirror units). While the requirements are still at an early stage, the phasing and diagnostic station is also expected to have demanding performance requirements related to the primary mirror phasing. Other constraints such as the mass, design and access volumes also provide important constraints on the system. The next phase of the system development will include detailed design of the PFS-A Main System and hosted units: Wavefront Sensing and Imaging Camera Systems, and Hosted Metrology. The Phasing and Diagnostic Station and its camera systems will be the subject of a test-bench development phase known as MELT [6] before entering its detailed design phase.

## REFERENCES

- [1] "The E-ELT Construction Proposal", [http://www.eso.org/public/archives/books/pdf/book\\_0046.pdf](http://www.eso.org/public/archives/books/pdf/book_0046.pdf)
- [2] Noll, R.J., "Zernike polynomials and atmospheric turbulence," J. Opt. Soc. Am. 66, 207-211 (1976)
- [3] Jolley, P., Brunetto, E., Frank, C., Lewis, S., Marchetti, E., "Prefocal station mechanical design concept study for the E-ELT," Proc. SPIE 9906, Ground-based and Airborne Telescopes VI, 99062H (2016)
- [4] La Penna, P., Förster A., Frank, C., Guidolin, I., Guisard, S., Hammesley, P., Holzlohner, R., Jolley, P., Kosmalski, J., Lampater, U., Lewis, S., Marchetti, E., "ELT Pre-Focal Station NGS Sensor Arm," Proc. AO4ELT5, (2017)
- [5] Reyes, J., et al., "An overview of the ESO adaptive optics wavefront sensing camera," Proc. SPIE 8447, 237 (2012)
- [6] Pfrommer, T., et. al., "The optomechanical realization of a minuscule Extremely Large telescope, MELT, for wavefront control, phasing, and telescope control algorithm test scenarios," Proc. SPIE 10700-123 (2018)
- [7] Holzlohner, R., Kellerer, A., "SENSITIZER", <https://www.eso.org/sci/facilities/develop/software.html>